Master's Thesis of Science

Determining the Optimum Conditions for Generating Fine Topography in Tidal Flats Using an In-SAR System

갯벌 지형도 생성을 위한
최적화된 In-SAR 시스템 결정

August 2017

Graduate School of
Earth and Environmental Science
Seoul National University

Changhyun Choi

Abstract

Continuous monitoring of the topographic heights and changes in tidal flats has been important but extremely challenging. It is generally difficult to observe the change of tidal flat topography from only on-site measurements. In this regard, interferometric synthetic aperture radar (In-SAR) measurements can be an effective strategy to generate precise DEMs and detect large-scale topographic changes. Nevertheless, utilizing interferometric synthetic aperture radar to detect topographic change in tidal flats is not practical because the average slope of tidal flats is usually less than a degree and the overall spatial height variation is less than 5 m. Besides, the temporal height variation is small requiring long observation periods. Therefore, the accuracy of In-SAR DEMs must be especially high to detect meaningful topographic variation. In order to minimize the error of In-SAR DEMs, height of ambiguity (HoA) and random phase deviation of interferogram should be taken into account. These two factors are related to incidence angle as well as baseline. In this study, we investigate topographic error level in tidal flat when using single-pass In-SAR system. Phase deviation of interferogram is derived by conventional geometry and equations. SNR and geometric decorrelation is expressed by function of baseline as well as incidence angle. The result shows that height error of DEM is minimized to be less than 15 cm when baseline is 1500 m with an

incidence angle of 29˚ in TanDEM-X system. Finally, validation of the model was carried out by comparing with TanDEM-X interferograms out which is the only single-pass interferometric satellite mission carrying on SAR sensor. Finally, deposition and erosion pattern of Gomso bay was analyzed from difference of TanDEM-X DEMs.

Keyword: SAR Interferometry, Topography, Decorrelation, Tidal flat
Student Number: 2014-22434

Table of Contents

Figure list

Table list

1. Introduction

Tidal flats have provided economic profits to human communities and played a key role in Earth's ecosystem such as defending against storm surges and flooding, and providing productive habitats for fin-, shellfish, migratory birds, etc… [1-3]. However, observations of tidal flats reduction due to reclamation and sea level rise caused by climate changes have been inspiring world-wide concerns [4-7]. These changes can cause significant responses on both the human and ecology as consequence [8]. Recent reports indicated that coastal regions are under high stress, yet how manage human activities for conserving coastal region are never answered by governments or coastal science communities [2, 6, 9]. Thus, periodic monitoring of tidal flats topography is necessary to identify the response between land and sea also, possible to provide the way to manage coastal development [10].

Measurement of tidal flat topography is notoriously difficult, because the tidal flats are exposed only at low tide and on-site accessibility is extremely limited. These limitations have resulted in relatively few investigations and comprehensive reports on tidal flats [11]. Thus, there have been several trials to monitor its topography by generating time-series topography maps, also known as digital elevation model (DEM), using remote sensing data in coastal regions. Remote sensing has become an effective tool to monitor the tidal flats, especially able to achieve accurate and high resolution DEMs

[12, 13]. Waterline method is one of most common technique to generate DEMs over tidal flat [13-16]. Even though this method has an advantage because of low cost, quantitative analysis was limited because it cannot provide topographic information under the maximum tide level and it cannot reflect consequence of topographic change because it requires several scenes acquired at different periods with the topographic changes permeated within each scene. Light Detection and Ranging (LiDAR) system is another remote sensing technique to provide the topography in high precision [17]. However, the spatial resolution of LiDAR is on reciprocal proportional relationship with swath of system. Therefore, it is not effective way to observe coasts with large spatial coverage. There needs a system to overcome those limitations to provide a topography map so that the generated map does not contain additional errors due to temporal changes and has a large spatial coverage with high resolution.

Recently, interferometric synthetic aperture radar (In-SAR) system is believed to be one alternative system that is capable of doing so in tidal flats [18-20]. However, there exist two obstacles to produce the high accurate topography of tidal flats in general repeat-pass In-SAR system. First, due to the active tidal processes, the scattering features at each data acquisition dramatically are modified. These dramatic changes in the terrains are non-coherent, causing serious temporal decorrelation effect in In-SAR pairs. It makes multi-pass SAR interferometry not suitable in tidal flats [21]. This problem can be overcome by using a single pass interferometry system,

which is not affected by temporal decorrelation. Secondly, the average slopes of tidal flats are usually less than a degree with the spatial height variation is usually less than 5 m [18]. Also, the temporal height variation in tidal flats vary with local circumstances but usually less than few cm per day [22, 23]. Thus, we have to generate DEM with accuracy better than 10 cm in order to detect the topographic change in monthly scale.

In order to minimize the uncertainty of In-SAR system, we should consider two factors of interferometric SAR, height of ambiguity (HoA) and random phase deviation of interferogram. These factors are controlled by two geometric parameters. One of major factors of In-SAR topography error is baseline. Generally, a precise DEM extracted by In-SAR technique requires long perpendicular baseline between SAR sensors that could achieve small height of ambiguity. But if the baseline is too long, serious decorrelation will occur. Incidence angle as well as baseline are major parameters of a system. Incidence angle is related to resolution of SAR images and the range to a target. In-SAR measurement usually contains more error factors such as signal noise, volume decorrelation, temporal decorrelation and atmospheric phase screen effect. However, in a case of single-pass In-SAR system, most of coherent errors become negligible except thermal noise error and geometric decorrelation.

The main purpose of this study is determining the optimum conditions of In-SAR geometric parameters. In this study, we tried to simulate the coherence and height error level of In-SAR topography in tidal flats to find

relationship between sensitivity and two parameters. In Section Ⅱ, we briefly describe the relationship between coherence and two crucial parameters, incidence angle and baseline. The estimation is established from simplified conventional theoretical equations based on In-SAR geometry of [24]. Then, Section Ⅲ, we will describe the datasets, TanDEM-X pairs and the accurate Real Time Kinematic Global Positioning System (RTK-GPS) measurement that were used in this study and the study area. In Section Ⅳ, we will discuss about the simulation result of this study and try to determine the optimum state of system based on the simulation result. Then, in order to validate the model, comparison result was provided. Finally, we discussed about the result and its meaning.

2. Method

2.1. Theoretical Analysis

The DEM derived from In-SAR technique always has an uncertainty. According to Rodriguez and Martin [25], three kinds of error in In-SAR topographic height can be identified: (1) random error (2) geometric distortion and (3) positioning error, these three can explain most of height error. However, in this study, we assume that geometric distortion error and positioning error is totally compensated by the post-processing. We focused on random error, which depends on geometric parameters of radar interferometer system. In addition, it can be quantitatively estimated by using the relative height error. The relative height error H_{error} is derived as follows [26-28]

$$H_{error} = H_a \cdot \sigma_\phi / 2\pi \tag{1}$$

where H_a is height of ambiguity (HoA) and σ_ϕ is phase standard deviations of interferogram. HoA means topographic height difference between every 2π phase cycle in interferometric phase. HoA H_a is defined as follows [9, 11]

$$H_a = p \cdot \lambda r_{slant} \sin\theta_i / B_{perp} \tag{2}$$

where λ is wavelength of radar system, r_{slant} is slant range to target, θ_i is incidence angle, B_{perp} is perpendicular baseline between two sensors and p is constant that determined by mode of SAR acquisition, $p = 1/2$ for mono-static and $p = 1$ for bi-static mode. The wavelength of radar system cannot be controlled in the imaging acquisition but baseline of single-pass In-SAR system became a flexible to what extend through the development of present technology. These are key parameters that determine HoA as well as the distance to the target. We can represent that the HoA is simply governed by baseline and incidence angle.

Whereas, the deviation of interferometric phase is impossible to represent by simple equation, which is probability density function of coherence and numbers of looks. When multi-look window size is n, interferogram phase statistics can be described as following equation derived by Lee [29, 30]

$$P^{(n)}(\phi) = \frac{\Gamma\left(n+\frac{1}{2}\right)\left(1-|\gamma|^2\right)^n \beta}{2\sqrt{\pi}(1-\beta^2)^{n+\frac{1}{2}}} + \frac{\left(1-|\gamma|^2\right)^n}{2\pi} \cdot \ {}_2F_1\left(n, 1; \frac{1}{2}; \beta^2\right), -\pi < \phi \leq \pi \tag{3}$$

where

$$\beta = |\rho| \cos \phi. \tag{4}$$

where coherence γ from the normalized complex correlation coefficient between master and slave signals. The coherence is the most important parameter in describing this function. Coherence of two complex SAR signal matrix Z_1 and Z_2 can is defined as follows [31]

$$\gamma = \frac{E(Z_1 Z_2^*)}{\sqrt{E(|Z_1|^2)E(|Z_2|^2)}} \tag{6}$$

where $E(x)$ means the ensemble average value of x and * means the complex conjugate. The random phase error can be calculated by

$$\sigma_\phi = \int_{-\pi}^{\pi} \phi^2 P^n(\phi) d\phi. \tag{5}$$

In order to obtain accurate topographic information, we have to determine the In-SAR geometry, which is optimized to minimize the height error. Thus, in this section, we briefly described decorrelation factors and simplified to simulate with model. Then, based on these formulas, we tried to find relation between the key parameters, baseline and incidence angle, and height error inferred from In-SAR.

2.1.1. Decorrelation factors

As we mentioned, coherence is the important parameter to evaluate quality of an interferogram [28]. Generally, coherence means the magnitude of complex coherence |γ|, which is located in 0 to 1. There exist various decorrelation effects to reduce the correlation between two signals. Decorrelation effect can be divided into mainly four factors, SNR, geometric, volumetric and temporal decorrelation [26, 27]. The total decorrelation value γ_{total} can be expressed as follow

$$\gamma_{total} = \gamma_{SNR}\gamma_{geometric}\gamma_{volumetric}\gamma_{temporal}. \quad (7)$$

However, active tidal process alters scattering particles or dielectric features on the surface. It generates serious temporal decorrelation in every tide period. Therefore, single-pass system is the only alternative way to preserve the reliable topographic phase on tidal flats. Thus, we can assume that the temporal decorrelation is negligible in case of tidal flat. Additionally, surface scattering is dominant in this kind of terrain because their very high soil moisture and conductivity blocked penetrating of microwaves [32]. In this point, we can also consider that volumetric decorrelation is neglected. Then, only two decorrelation effects was remained what we should concern in tidal flats, SNR and geometric

decorrelation

$$\gamma_{tidal\ \ flat} = \gamma_{SNR}\gamma_{geometric}. \quad (8)$$

2.1.2. SNR decorrelation

SNR decorrelation is caused by thermal noise of the sensors. SNR decorrelation γ_{SNR} can be described as follow [26, 27, 31]

$$\gamma_{SNR} = \frac{1}{1+SNR^{-1}}. \quad (9)$$

SNR decorrelation is one of the important decorrelation in coastal region because backscattering intensity is not enough strong to make SNR decorrelation negligible. In the previous, we can consider tidal flat is surface scattering dominant thus the IEM model is suitable for describing the backscattering of this kind of surface [32]. IEM, proposed by Fung and Chen [33], can estimate the normalized radar cross section (NRCS) of bare soil as a function of its dielectric constant, vertical surface roughness and correlation length. Dielectric constant is estimated using Dobson's [34] equation which is the measured relationship between dielectric constant and soil moisture experimentally. However, we do not have enough information about surface roughness parameters. Therefore NRCS histograms, extracted from TanDEM-X SAR images with various incidence angles, were used in order to estimate roughness parameters. NRCS variation is affected to tilting direction toward radar as well as surface roughness parameters. However, we can find the high backscattering at various

regions not only around channel but also relatively flat area. Thus, we assume that mean backscattering coefficient corresponds the mean surface roughness of each coastal region.

Then, we tried to determine the relationship between incidence angles and mean backscattering coefficient. This method was completely empirical approach. We determine the range of roughness parameter then, at each candidate parameter, IEM model was applied to predict the theoretical curves of incidence angle and backscattering coefficient. Finally, SNR function of incidence angle was computed based on both derived IEM model and reference noise information. The processing step of SNR estimation is illustrated in Fig. 1.

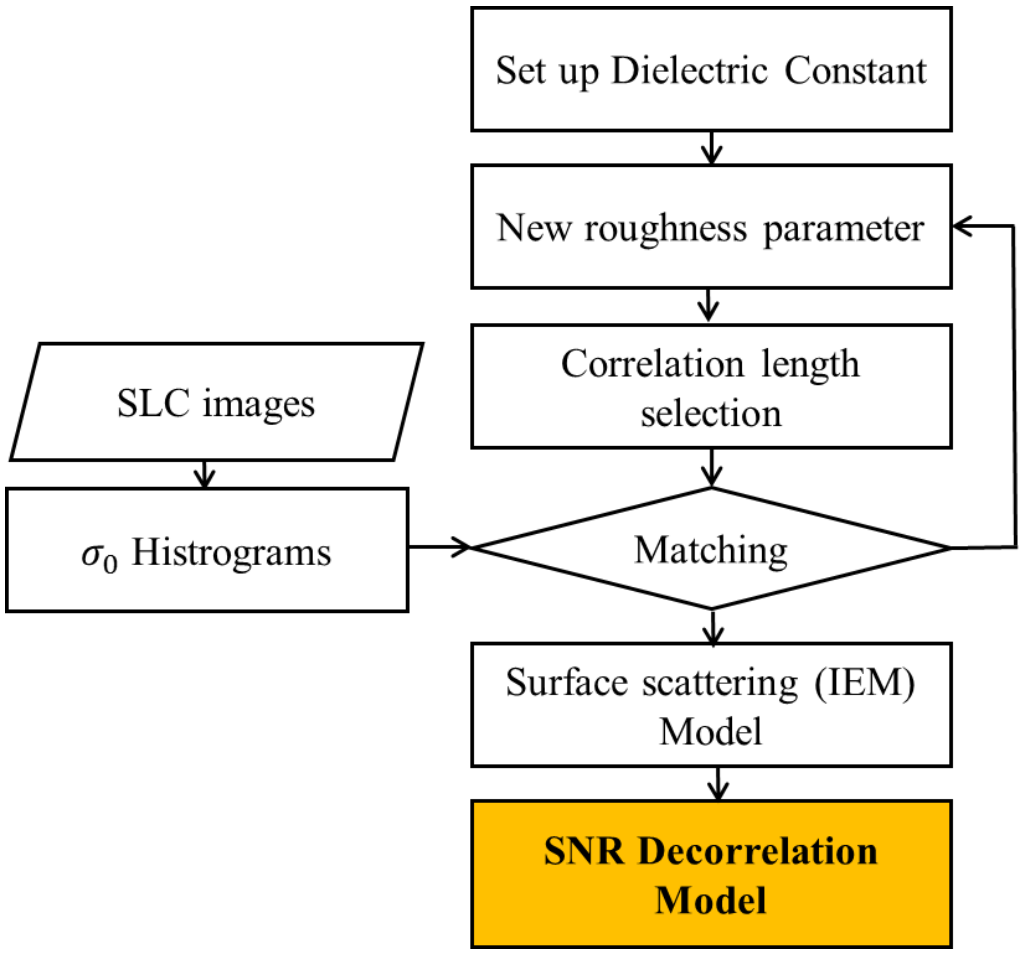

Fig. 1. Processing step to estimate SNR from IEM curve fitting.

2.1.3. Geometric decorrelation

Geometric decorrelation was caused by spectral shift from angular separation [35]. Geometric decorrelation function as the result of the phase offset due to baseline can be described by [26, 27]

$$\gamma_{geometric} = 1 - \frac{2R_y B_{perp} \cos\theta_i}{\lambda r_{slant}} \tag{10}$$

where θ_i is incidence angle, R_y is range resolution, B_{perp} is effective baseline and r_{slant} is slant range to target. In general satellite system case, equation of $\gamma_{geometric}$ can be modified by Lee and Liu [36]

$$\gamma_{geometric} = 1 - \frac{cB_{perp} \cot(\theta_i - \alpha)}{B_w \lambda r_{slant}} \tag{11}$$

where c is the speed of light, B_w is frequency bandwidth of system and local terrain slope α. The average terrain slope α is almost 0°. Thus, Eq. (11) is approximated by

$$\gamma_{geometric} = 1 - \frac{cB_{perp} \cot(\theta_i)}{B_w \lambda r_{slant}}. \tag{12}$$

Finally, assuming that earth is sphere then, we can derive the slant range

from geometry. The derived equation is

$$r_{slant} = -R_e \cos\theta_i + \sqrt{R_e^2 \cos^2\theta_i + hR_e + h^2} \qquad (12)$$

where h is height of satellite orbit and R_e is earth radius. The slant range to target r_{slant} is function of the incidence angle. Since the other parameters that the speed of light, wavelength(X-band channel) and bandwidth is constant in SAR system, this means the geometric decorrelation function is in terms of only the baseline and incidence angle. Therefore, combining two equations of SNR decorrelation and geometric decorrelation (Eqs. (9 & 12)), decorrelation function of tidal flats is in relation with baseline and incidence angle. We simulated DEM error derived from In-SAR based on these equations then, compared with measured one.

2.2. Study area and Dataset

In order to validate the simulation result and robustness, we acquired SAR data and GPS measurements nearly same time. Currently, the only way to obtain single-pass space-borne SAR data is by TanDEM-X system. In this study, TanDEM-X data acquisition and in-situ measurements performed in the year 2015 and 2016 over study area.

2.2.1. Study area

We chose Doowoori tidal flat as study site shown in Fig. 2. The main reason for this choice is accessibility. It is located at the mouth of Hampyong bay in the Western Korea peninsula. Around coastlines are hard to survey because of their hostile environments and its tide level change. The Hampyong bay is the meso-tidal region where has 3.47 meter of average sea level variation with semi-diurnal tide [37]. The Korea climate is under effect if typical monsoon of East Asia. Thus, there are seasonal variation is significant factor including Hampyong bay. However, the most important feature of Doowoori is relatively small seasonal variation of height [38]. For this reason, even though there exist time interval between In-SAR data acquisition and in-situ measurements, we can estimate DEM error level by only comparing the reference GPS data with DEM inferred from TanDEM-X in the Doowoori tidal flat.

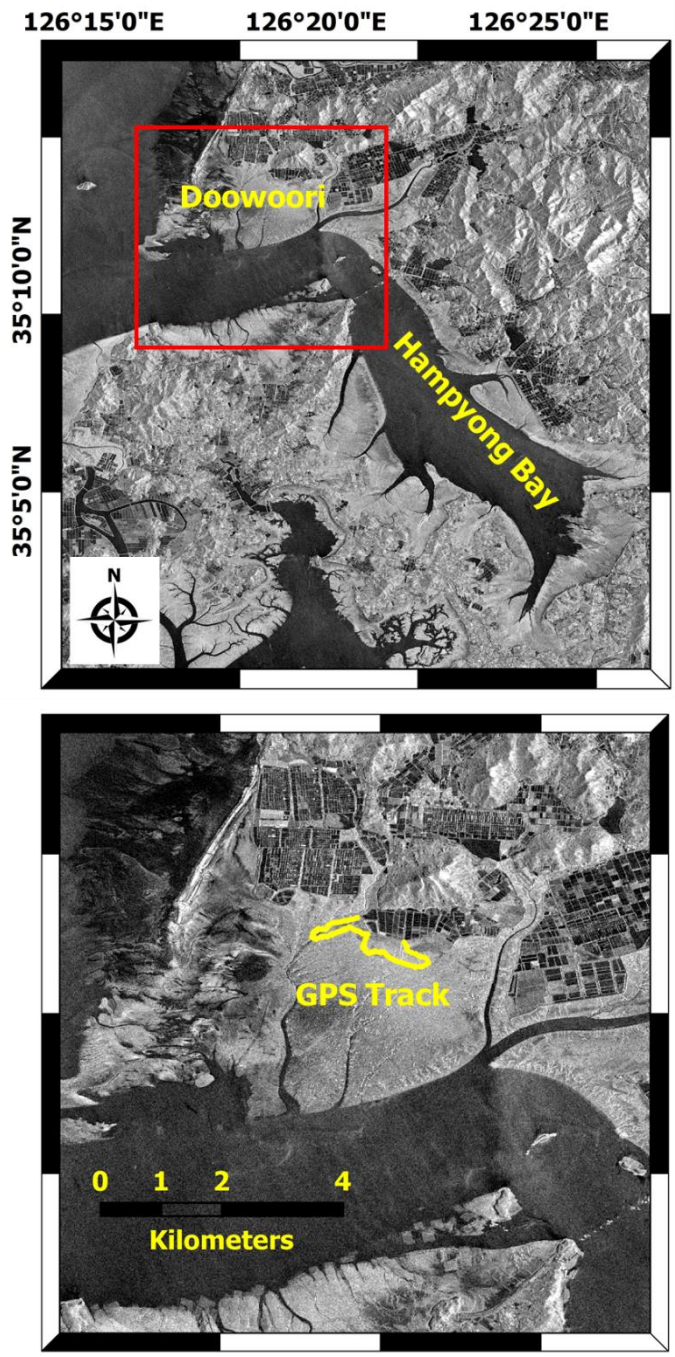

Fig. 2. TanDEM-X image of study area “Hampyong Bay” located in western Korean peninsula. Mixed mud flat with high concentration of silt is dominant on the surface.

2.2.2. TanDEM-X SAR data

TanDEM-X is the first twin satellite system with TerraSAR-X. Both satellites carry-on same SAR sensors are able to perform a bi-static mode [39]. Those imaging radar sensors operate at X-band (9.65 GHz) with full polarization and perform in several beam modes including strip-map mode, wide-swath mode and high-resolution mode. The range of incidence angle is 20 to 50 degree and the range of effective baseline is 0 m to 2000 m. Pixel spacing resolution of image (is around 2 m in strip-map mode) depends on the beam mode, incidence angle and beam width.

In this study, the seven image pairs in bi-static strip-map mode were acquired for the analysis. We used the images which have range of incidence angle is 28 to 45 degree. Six images were acquired with HH-polarization and the other image was VV-polarization. Four images have 100MHz beam width rest images have 150MHz. Fig. 2 is the TanDEM-X image acquired in 12th June 2015. We applied the typical In-SAR processing method to extract DEMs for each image pair. From each image, we chose a site to evaluate the accuracy of each extracted DEM. Test site is Doowoori tidal flat located at open coast of Hampyong bay. The main reason for this choice is accessibility. Around coastlines are hard to survey because of their hostile environments and its tide level change. TanDEM-X data were acquired in December 2012 to September 2015 and the ground

measurement was conducted in December 2015 and January 2016. The tide levels are provided from Korea Hydrographic and Oceanographic Agency (KHOA). The detail description of SAR data was noted in the table I.

Table 1. Specifications of TanDEM-X SAR data and the tide level

Acquisition Date (YYYY/MM/DD)	Perpendicular Baseline	Incidence Angle	Bandwidth	Polarization	Tide Level
2012/12/08	171 m	34.7°	100 MHz	HH	298 cm (Flood)
2014/09/05	13 m	44.5°	100 MHz	VV	202 cm (Ebb)
2015/06/12	1280 m	29°	150 MHz	HH	178 cm (Flood)
2015/08/12	1077 m	44.5°	100 MHz	HH	292 cm (ebb)
2015/08/14	1315 m	33.5°	150 MHz	HH	270 cm (Ebb)
2015/09/08	974 m	28.8°	150 MHz	HH	235 cm (Ebb)
2015/09/25	547 m	44.5°	100 MHz	HH	170 cm (Ebb)

2.2.3. In-situ measurement

Reference height information is also necessary to determine absolute height of DEM since we also obtained the several data around the study area to determine absolute height of DEM the ground measurement was conducted in December 2015 and January 2016. The tide levels are provided from Korea Hydrographic and Oceanographic Agency (KHOA). The detail description of SAR data was noted in the table I. RTK-GPS measurements. The obtained GPS tracks are depicted in Fig. 2. GPS measurements were conducted carefully to get precise information as reference with Leica Viva RTK-system. It has vertical accuracy of 2 cm. We used a GPS pole (2m length) to reduce the interference and multiple reflections. The balance of the pole was continuously checked by bubble inside of its handle. Moreover, the pole was supported on a flat board on the mud to prevent from sinking. All elevation data of DEM and GPS were converted into the WGS-84 ellipsoid to compare heights because some DEM data such as SRTM use EGM96 geoid.

Fig. 3. RTK-GPS measurement of tidal flat surface using Leica viva system.

2.3. Data Processing

DEMs are generated using typical SAR interferometry technique. Level 1 SAR data were collected from DLR. From the co-registrated images, we calculate interferograms. WGS84 reference ellipsoid was subtracted from interferograms to acquire flattened images. Then, the images are masked out with the threshold of less than coherence 0.5. These interferograms are unwrapped using MCF algorithm. After flattening process, we had to input the ground control points (GCPs) provided by National Geographic Information Institute (NGII) and RTK-GPS data in order to convert unwrapped phase to the absolute height and to calculate the revised baseline information. The extracted DEMs were geocoded and resampled by 15 m spatial by 15 m resolution. The processing step of DEM extraction is illustrated in Fig. 3.

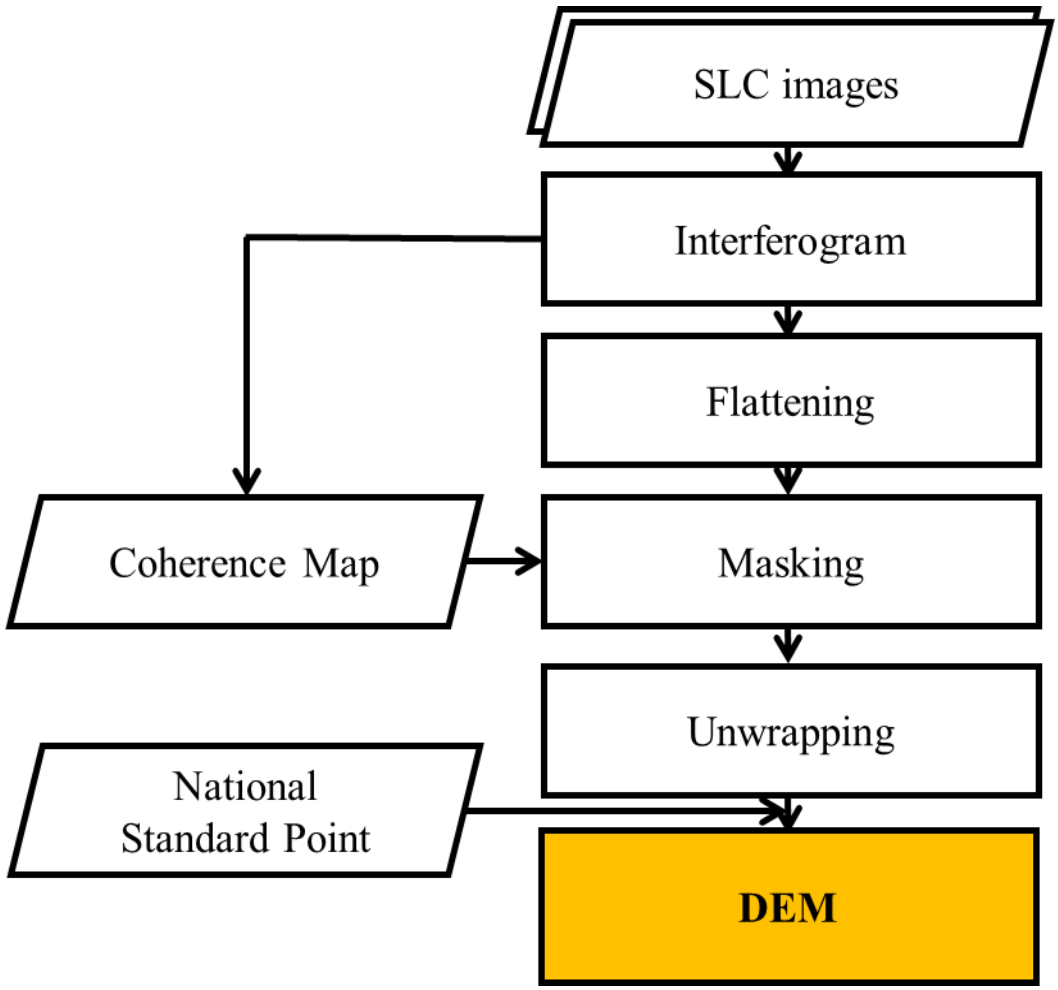

Fig. 3. Flow chart of Processing of SAR interferometry to generate DEM

3. DEM accuracy estimation

In this section, we proposed height error simulation ith function of baseline and incidence angle. The approach to simulate was described in Section Ⅱ. Also, we validated our simulation results by using interferograms derived from TanDEM-X data. The used interferograms are generated by the GAMMA software.

3.1. Simulation Result

3.1.1. SNR simulation

By simulating the IEM model by using TanDEM-X NRCS histogram, we could figure out the NRCS function in term of incidence angle in tidal flats. In addition, we can obtain the information of surface roughness parameters. Estimated parameters from the curve fittings were RMS roughness 0.45 cm and correlation length 10 cm. This value is in good agreement with the value from on-site measurements obtained by Choe [11]. Then, noise equivalent sigma zero of TerraSAR-X was applied to calculate SNR decorrelation. The generated model curve and sigma naught histograms were depicted in Fig. 3. The depicted histograms are typical bimodal distributions. It is because of remnant water effect. In order to extract surface information, we should remove remnant water effect by Gaussian fitting. In Fig. 3 (a), the red points are mean value of each histogram extracted from TanDEM-X images. Fig. 3 (b) shows the generated SNR decorrelation function about incidence angle. As shown in the Fig. 3 (b), coherence dips as low as below 0.6 when incidence angle is 60 degree.

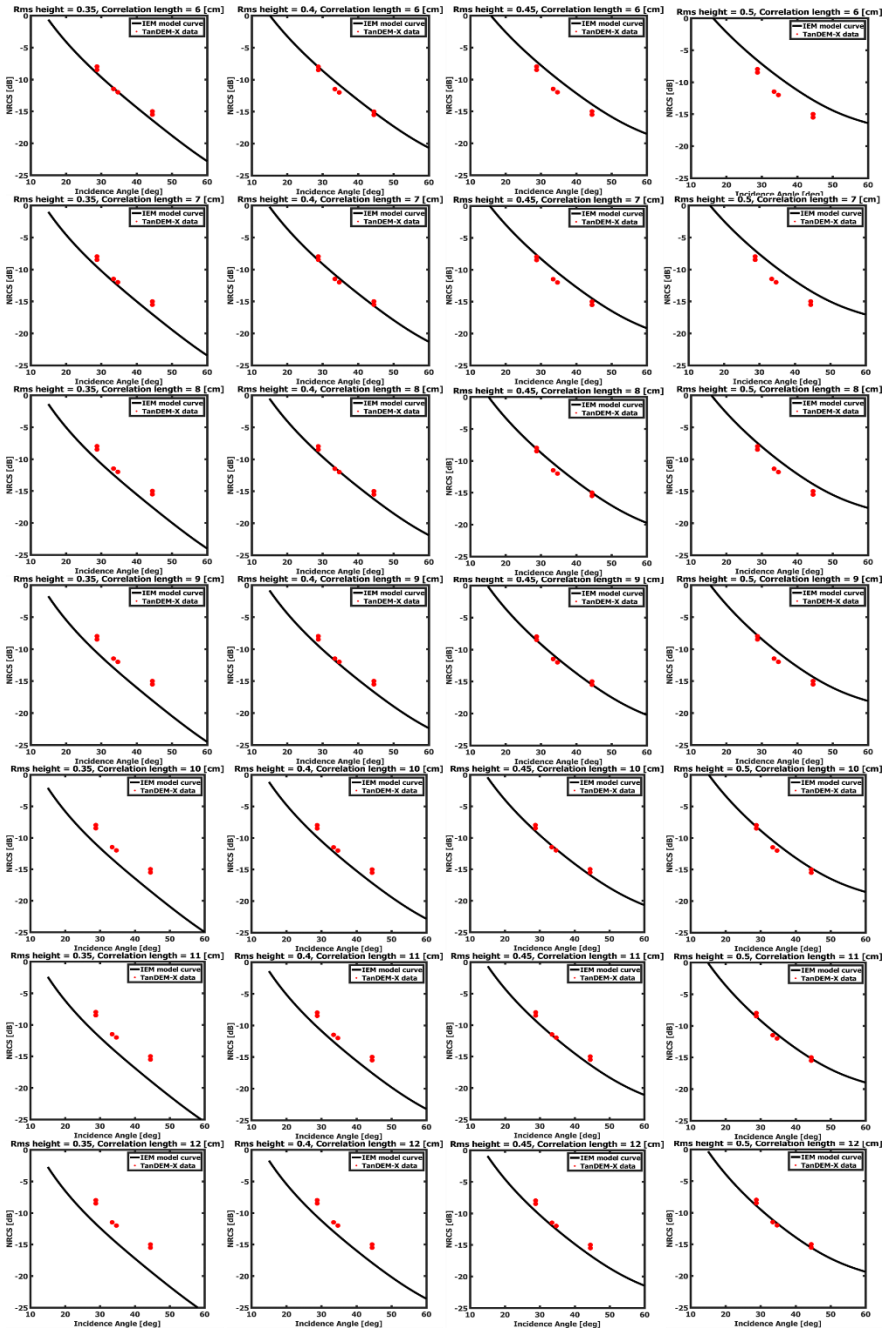

Fig. 4. IEM model curve fitting using TanDEM-X NRCS histogram. Surface RMS roughness varies in 0.35 cm to 0.5 cm and correlation length varies in 6 cm to 12 cm.

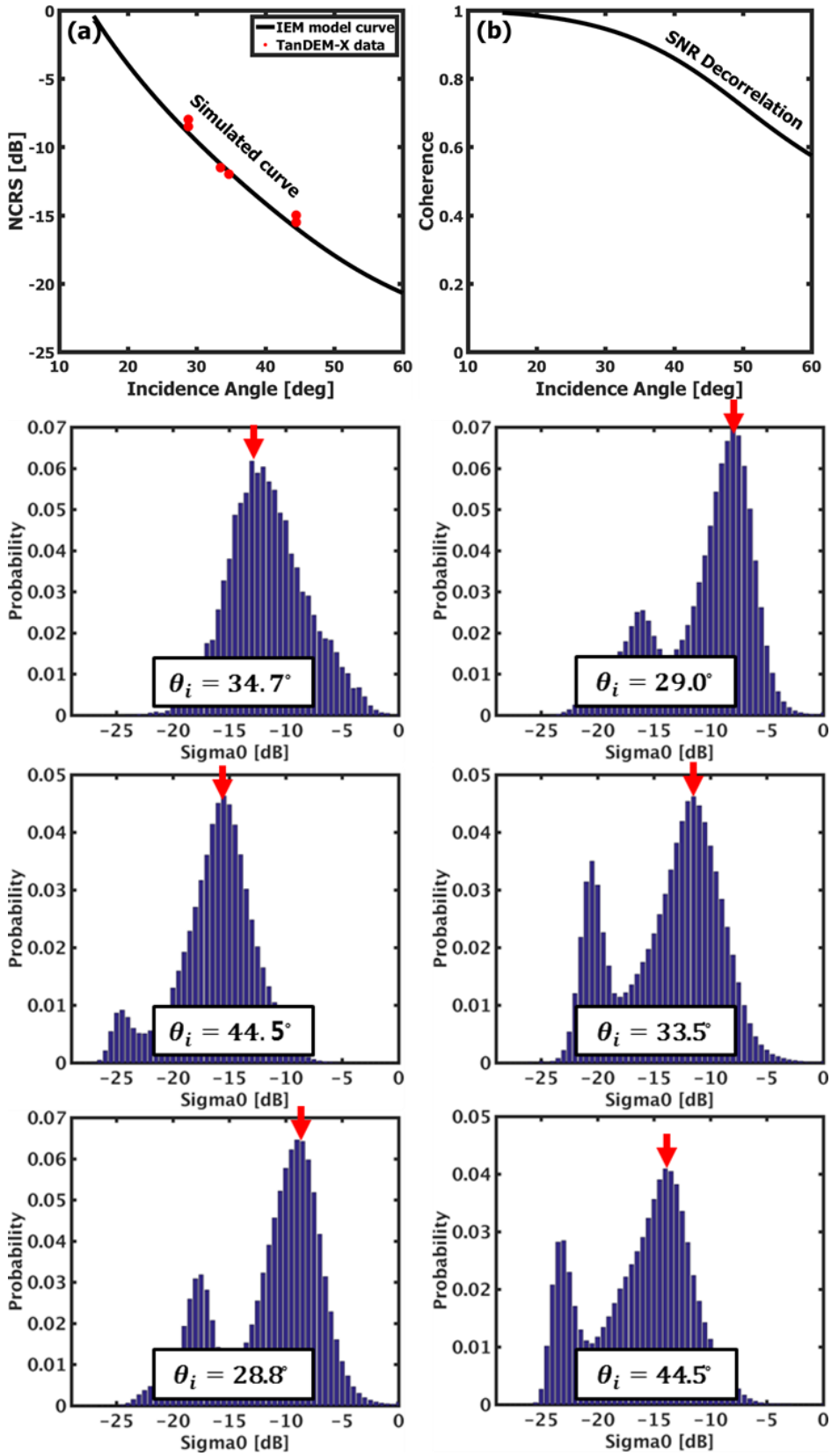
(a)
IEM model curve
TanDEM-X data
Simulated curve
NCRS [dB]
Incidence Angle [deg]
(b)
SNR Decorrelation
Coherence
Incidence Angle [deg]
Probability
Sigma0 [dB]
$\theta_i = 34.7^\circ$
$\theta_i = 29.0^\circ$
$\theta_i = 44.5^\circ$
$\theta_i = 33.5^\circ$
$\theta_i = 28.8^\circ$
$\theta_i = 44.5^\circ$

Fig. 5. The generated model curve and sigma naught histograms. All data were acquired in strip-map mode. (a) Simulated IEM model curve with reference NRCS data from TanDEM-X. Estimated RMS roughness is 0.45 cm and correlation length 10 cm. Simulation was conducted surface RMS roughness varies in 0.35 cm to 0.5 cm and correlation length varies in 6 cm to 12 cm. The red dots are extracted points from each histogram. (b) SNR decorrelation simulation result. This decorrelation was calculated by eq. (9).

3.1.2. Coherence & Height of Ambiguity Simulation

Then, coherence and HoA estimations were calculated at X-band, HH-polarization, 100MHz and 150MHz bandwidth in range of incidence angle 15 to 60 and baseline 100 m to 2000 m, which distributed in TanDEM-X data configuration range. Fig. 6 shows (a) HoA and (b), (c) coherence behavior depend on baseline and incidence angle. HoA is independent with bandwidth. In Fig. 6 (a), we can see the HoA is getting smaller as baseline increase and incidence angle decrease. Coherence depends on bandwidth because spatial decorrelation is function of the bandwidth. We can see coherence in tidal flats is determined by SNR decorrelation and spatial decorrelation in eq. (8). As shown in Fig. 6 (b) & (c) coherence decreases as baseline getting longer because spatial decorrelation is also getting serious. However, regarding incidence angle, coherence has different behavior because both decorrelation are related to incidence angle.

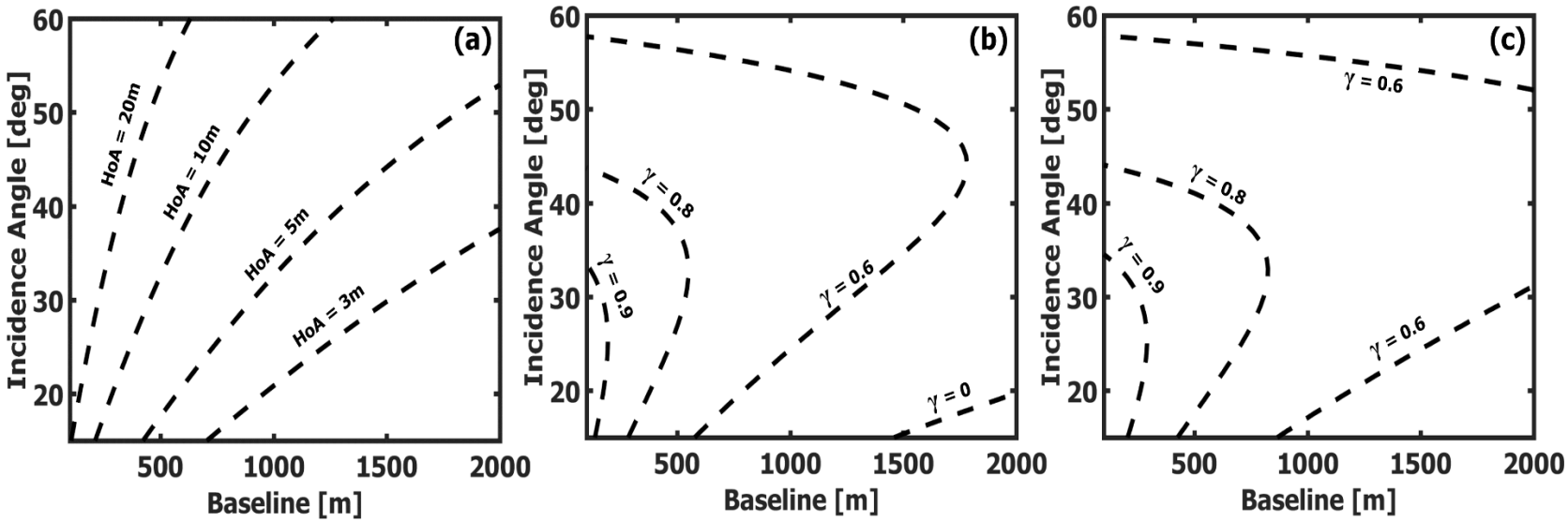

Fig. 6. Height of ambiguity and coherence function in baseline and incidence angle. (a) Height of ambiguity of system and (b) Estimated coherence when bandwidth is 100 MHz (c) Estimated coherence when bandwidth is 100 MHz.

3.1.3. In-SAR DEM Height Error Simulation in coastal area

Fig. 7 shows quantitative analysis of DEM error extracted from single pass In-SAR in tidal flat. Given baseline and incidence angle, we can predict relative height error as well as coherence or HoA. In 100 MHz bandwidth case, the interferogram totally lose its correlation in low incidence angle (less than 20 ˚) and long baseline (larger than 1500m). The important thing is relative height error has minimum point in range of incidence angle and baseline. In this simulation, we can find the lowest height error level is Fig. 7 (a) about 20 cm where baseline is around 880 m and incidence angle around 25˚ in 100 MHz bandwidth case, Fig.5 (b) about 14 cm where baseline is around 1315 m and incidence angle around 25˚ under 150 MHz bandwidth.

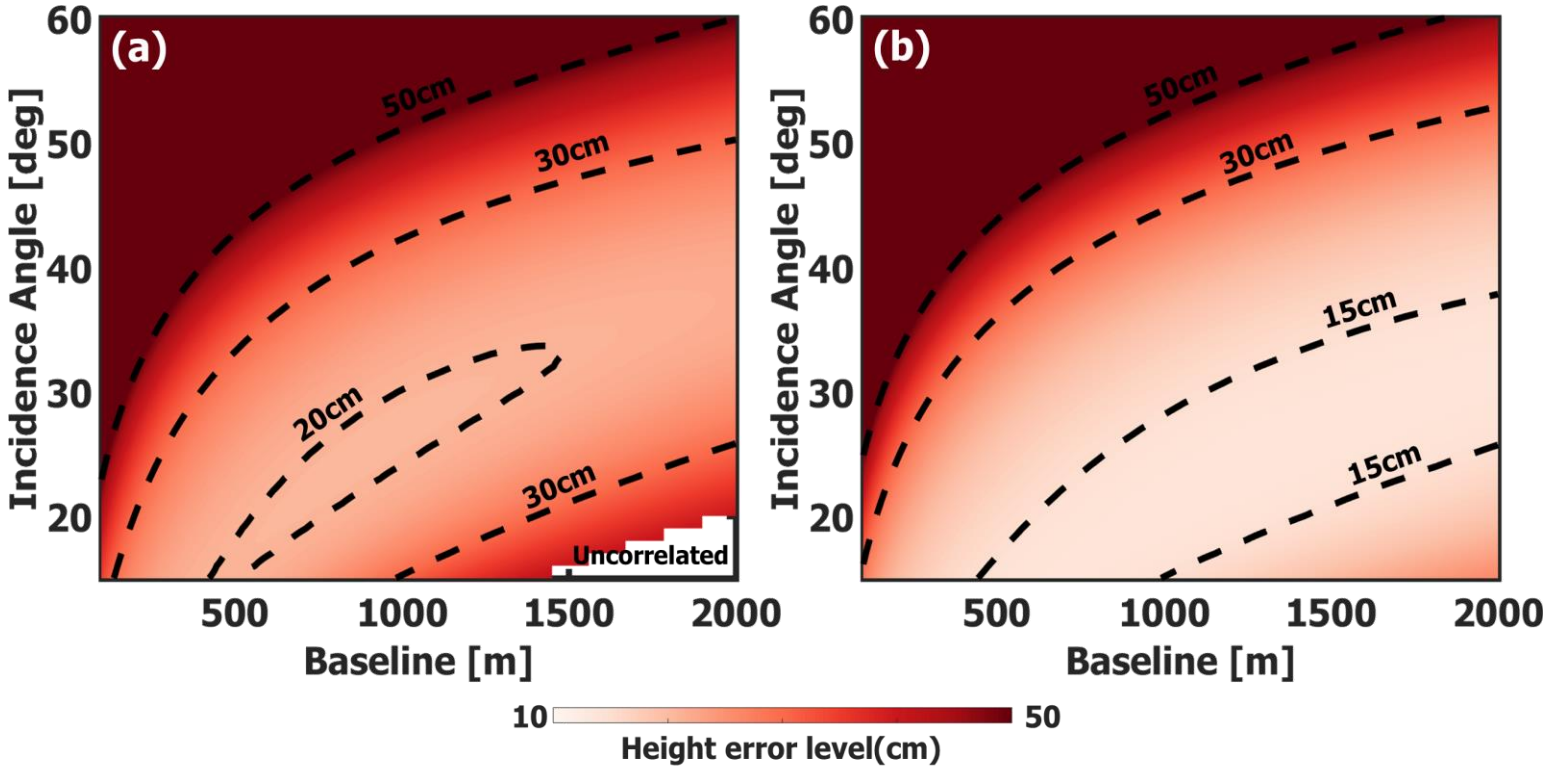

Fig. 7. Simulated height error map for TanDEM-X formation of strip-map mode. (a) 100 MHz bandwidth. (b) 150 MHz bandwidth. Dash lines indicated error level contour.

3.2. Determination of optimum condition

We calculated In-SAR topographic error in tidal flats in case of flat state. Then, we tried to confirm which condition is optimum to generate fine topography map with lots of detail. Tidal flats have many macro- and micro- structures with local slope. Thus, we also considered local slope of terrain to determine the best condition of In-SAR system that could preserve detail information of topography. In order to reflect fine topographic structure in coastal area, the interferogram have ability to adapt in local slope. In other words, to be effective system to generate DEM in coastal area, the system have not to lose almost of coherence at various kinds of local slope. Therefore, eq. (11) should be used to estimate error in dipping area. It also affects to SNR as well as NRCS value of scatter.

Fig. 8. shows this kind of decorrelation. Fig. 8 (a) represented $\gamma/(\gamma_{SNR} * \gamma_{spatial})$. In case of mountains, volume decorrelation is dominant because of included various vegetation. However, there is no significant volume scattering in coastal region. Thus, residual decorrelation is able to explain residual decorrelation due to local slope effect. This pattern is also well matched with terrain gradient in test site.

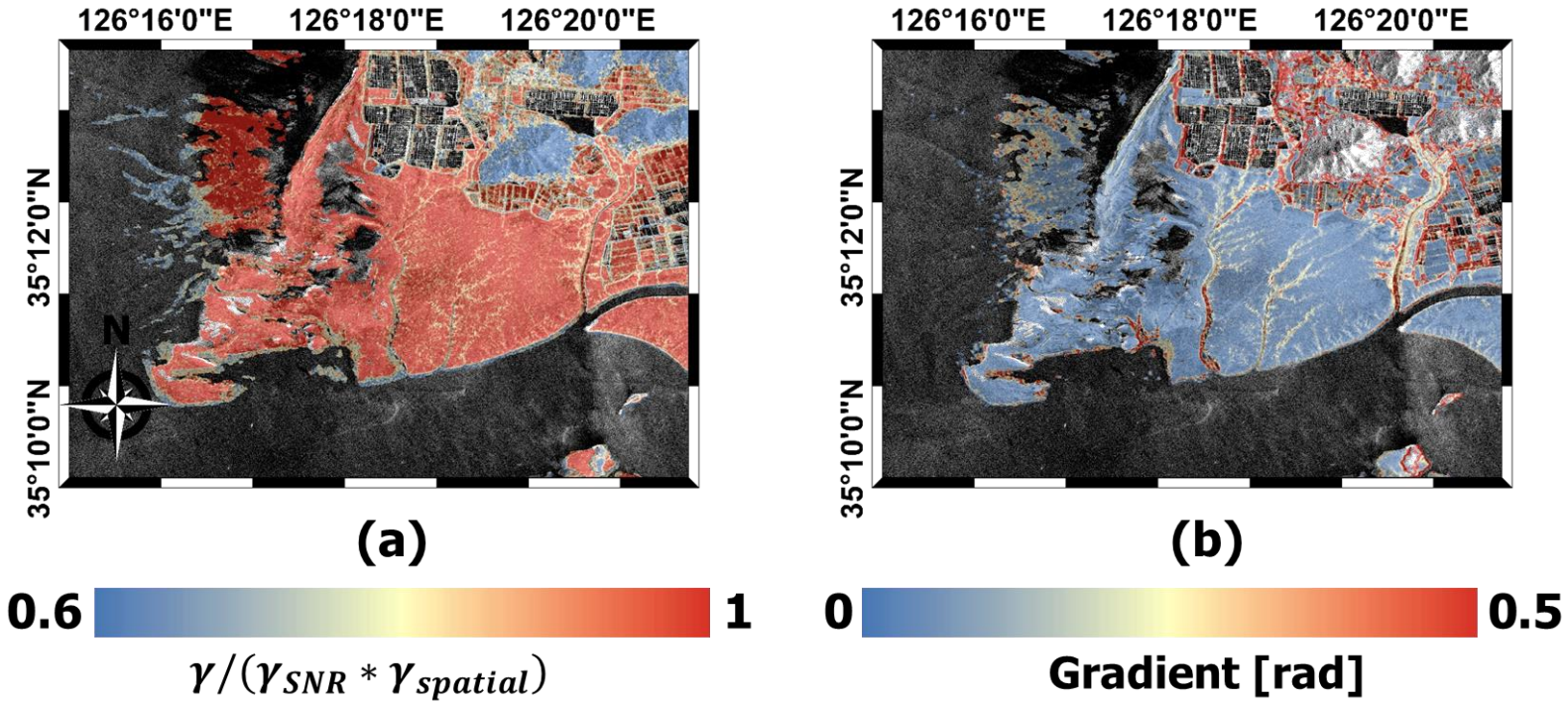

Fig. 8. (a) Decorrelation effect due to local slope and (b) terrain gradient calculated from DEM

Fig. 9. shows the simulated error level change of terrain slope variation. State of In-SAR formations are divided into 3 patterns, (1) small baseline with high incidence angle, (2) mid baseline with mid incidence angle and (3) large baseline with low incidence angle. The pattern (1) has a diametrically opposite shape with (3). When the local slope turn toward radar direction $(\alpha > 0)$, the former one [pattern (1)] gets more power of signal can cause decrease of SNR decorrelation. On the other hand, the latter one already has sufficient power from target. In this case, their geometric decorrelation is getting serious rather than SNR decorrelation decrease. Whereas when the local slope turn back on radar direction $(\alpha < 0)$, the former one [pattern (1)] lose their almost of signal can cause increase SNR decorrelation while pattern (3) maintains their signal with decrease of geometric decorrelation. Because of this local slope effect is possible to change the optimum range of In-SAR formation

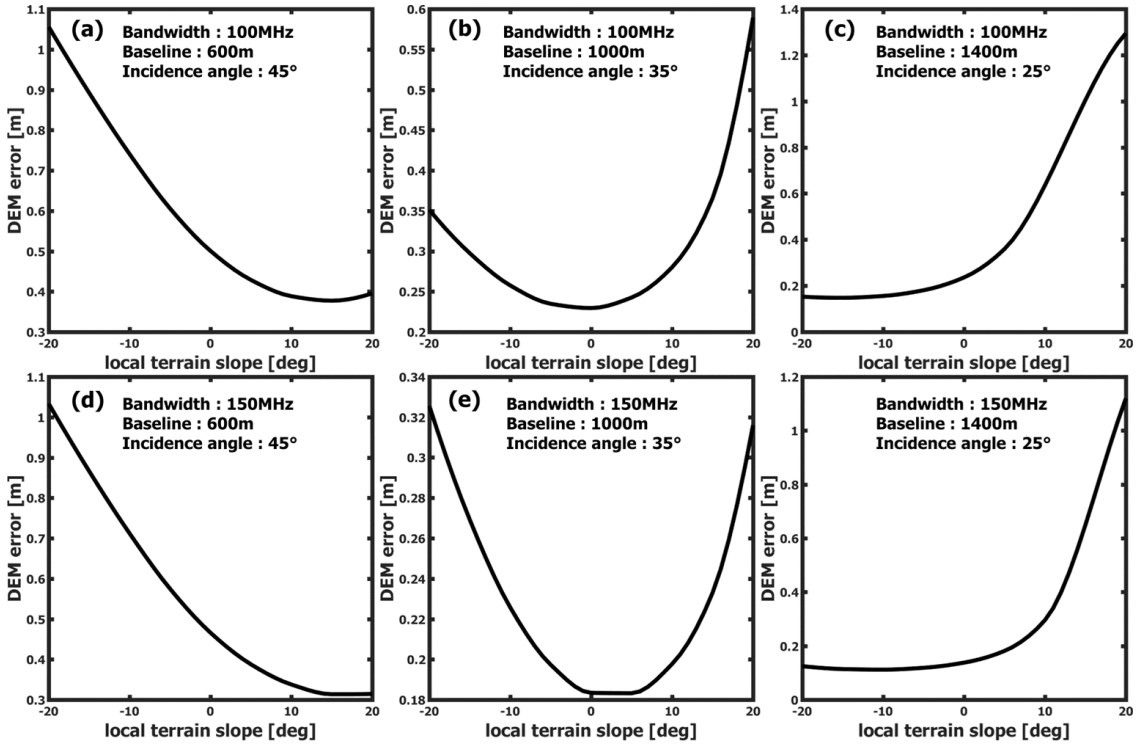

Fig. 9. The simulated height error change of local slope α variation. α is the local terrain slope angle from the horizontal plane towards radar direction. The each bandwidth, baseline and incidence angle is (a) 100MHz, 600m, 45° (b) 100MHz, 1000m, 35° (c) 100MHz, 1400m, 25° (d) 150MHz, 600m, 45° (e) 150MHz, 1000m, 35° and (f) 150MHz, 1400m and 25° respectively.

In order to estimate amount of decorrelation and its error, DEM accuracy was calculated at two directions, $\alpha = 5^{\circ}$ and $\alpha = -5^{\circ}$, which is the average absolute slope calculated from DEM. From these results, we calculate two more height error estimations in each state. Then, we made average error of flat state, upside slope ($\alpha > 0$) and downside slope ($\alpha < 0$). Fig. 8 shows the final estimation to determine the optimum system. The minimum error of 100MHz bandwidth is about 22 cm when baseline is 1080 m and incidence angle in 29 degree and the minimum error is about 15 cm when baseline is 1500 m and incidence angle in 29 degree.

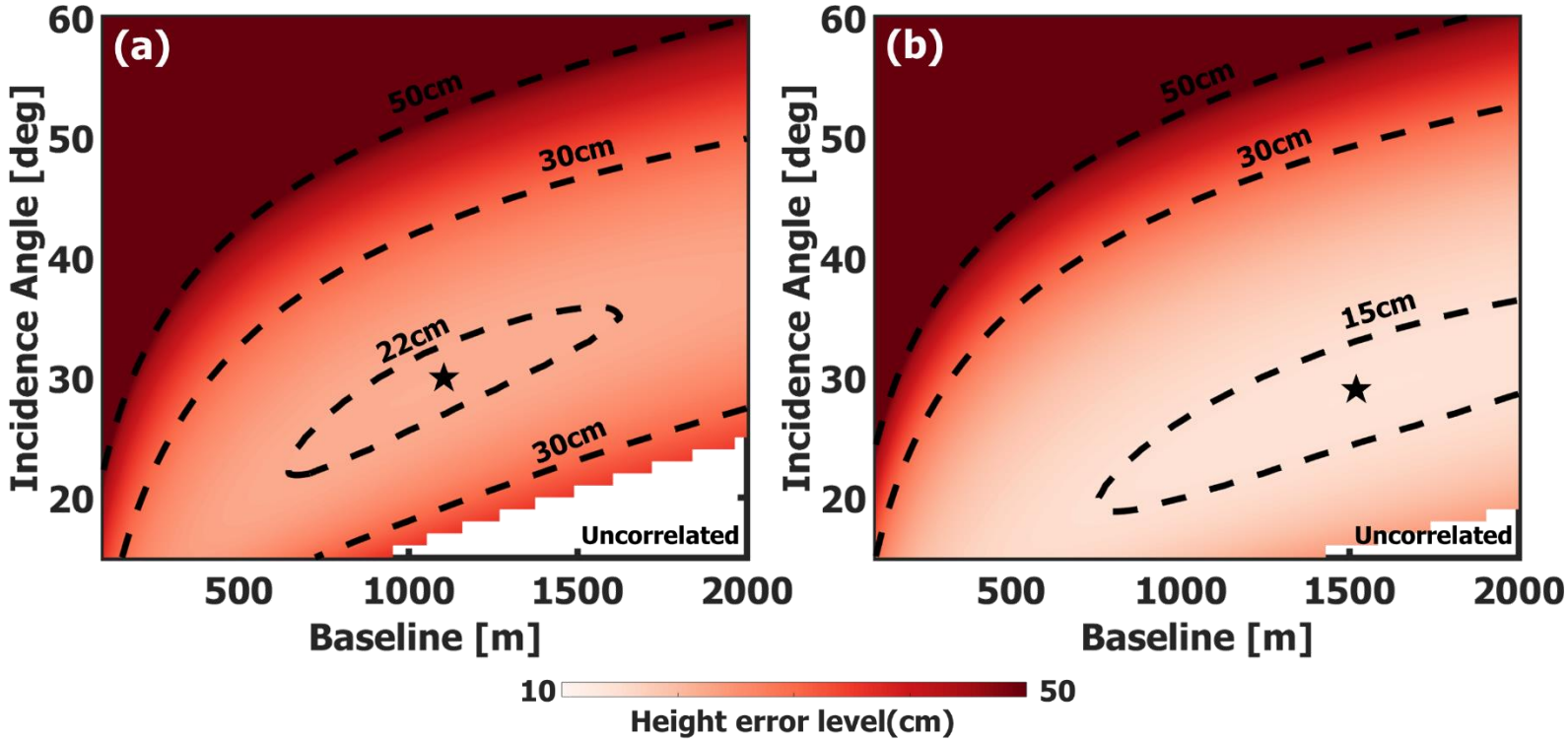

Fig. 10. Average simulated height error (a) 100MHz bandwidth (b) 150MHz bandwidth. ★ indicates the optimum state of In-SAR system, which is able to generate DEM with minimum height error.

3.3. Validation using TanDEM-X SAR data

In order to validate the model, we used the TanDEM-X interferograms to generate topography in study area with various baseline and incidence angle conditions. Additionally, geocoding was performed for every dataset in the same coordinate then, we extracted sigma naught and coherence histogram from each interferogram. From each pair we extracted the DEM in the study area. Fig. 11 shows the extracted topography, coherence and sigma naught map in 12th June 2015. Then, we compared the simulated value with calculated value from TanDEM-X data.

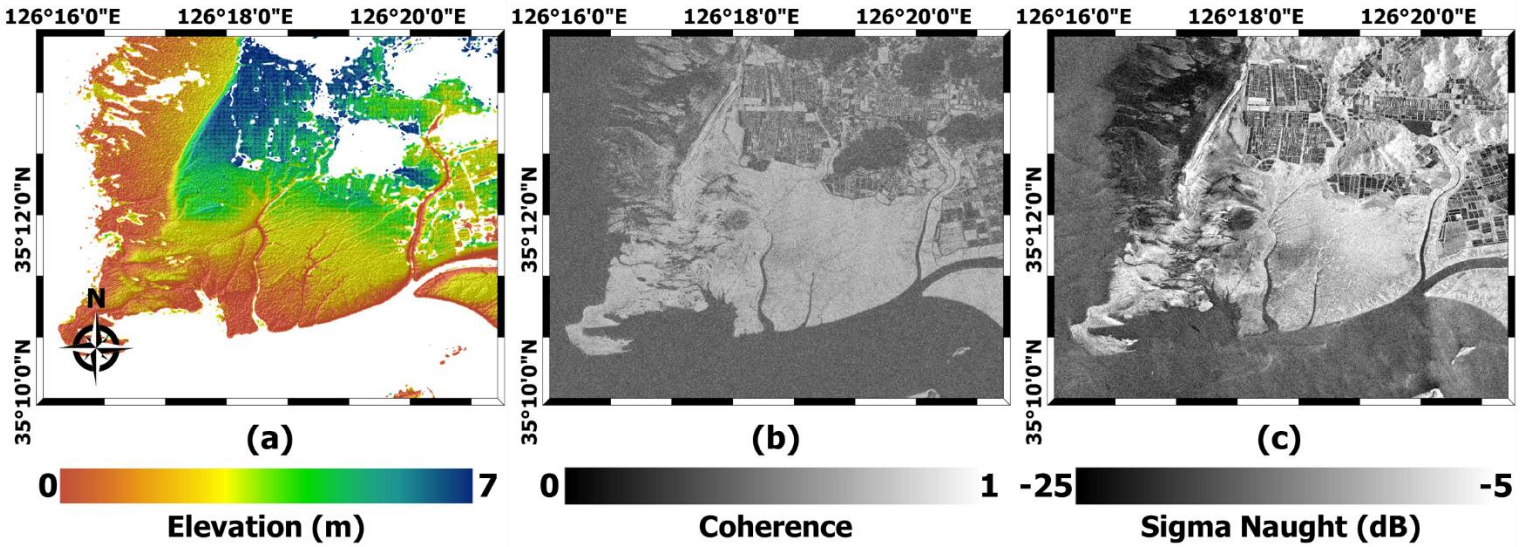

Fig. 11. The maps calculated from TanDEM-X data. (a) DEM. Topography map reflect many details in coastal area. For example, we can find the channel and sand bar formation. (b) Coherence map. The average coherence is 0.67 in Doowoori tidal flat. (c) NRCS map. The median sigma naught level in coast is -8.5 dB.

Comparison between GPS data and DEM provided RMS height error to us. In addition, we compared the simulated values, coherence and NRCS and the values extracted from TanDEM-X In-SAR datasets. For coherence, very long baseline with low incidence angle pairs (2015/06/12 & 2015/08/12 & 2015/08/14) have lower coherence than the others (2012/12/08 & 2014/09/05 & 2015/09/25) but their estimated error is much lower than other one. The estimated coherence and measured coherence have similar value in all case. Then, we compared the estimated height error level and measure data. We can find the tendency that height error level was under-estimated at long baseline pair. On the other hand, short baseline pair is well matched with estimated value. We can propose two possibilities (1) there is another bias error in interferometric DEM (2) long baseline and low incidence angle system is more vulnerable to slope variation than we expected or both factor can be existed simultaneously. Even we consider the bi-side slope effect; still estimated error is smaller than measured. Second hypothesis also could be derived the slope direction. Actual local slope do to be never limited only two kinds of direction, upward to sensor or downward to sensor. Then, the signal level will be lower than expected. The Table II shows the comparison result of the estimated value and extracted value from SAR data.

Table 2. Comparison between Simulated and Measured features of Interferogram

Acquisition Date (YYYY/MM/DD)	Expected Coherence	Coherence	Expected Height Error	Measured Height Error
2012/12/08	**0.92**	**0.90**	**0.73**	**0.68**
2014/09/05	**0.96**	**0.94**	**X**	**X**
2015/06/12	**0.71**	**0.67**	**0.15**	**0.27**
2015/08/12	**0.81**	**0.81**	**0.32**	**X**
2015/08/14	**0.76**	**0.74**	**0.17**	**0.26**
2015/09/08	**0.77**	**0.75**	**0.17**	**0.25**
2015/09/25	**0.88**	**0.88**	**0.55**	**0.35**

4. Application

Based on previous result, we tried to find the sedimentation pattern. In order to conduct quantitative analysis the sedimentation of tidal flat, Gomso bay is additionally selected for application. The reason why we chose that the study area is typical deposit dominant region [40] and there are many analysis for sedimentation rates [16, 40, 41]. Gomso bay is 8 km wide and 20 km long funnel-shaped, located in the western coast of Korea [16]. Previous studies provided the rates of deposit in Gomso bay is in slow rate of of 4~20 mm per month in mouth of the bay especially summer time [40] but around tidal bars have remarkable deposit rate with more than 20 cm per month [42]. In summer time, typhoons promotes erosion near the mouth of bay about few centimeter in every case.

We used two TanDEM-X pairs acquired in 12th June and 8th September 2015. Each pair has equal specification with Hampyong bay data because its orbit is same with the Hampyong bay one. We calculated DEM difference shown in Fig. 12.

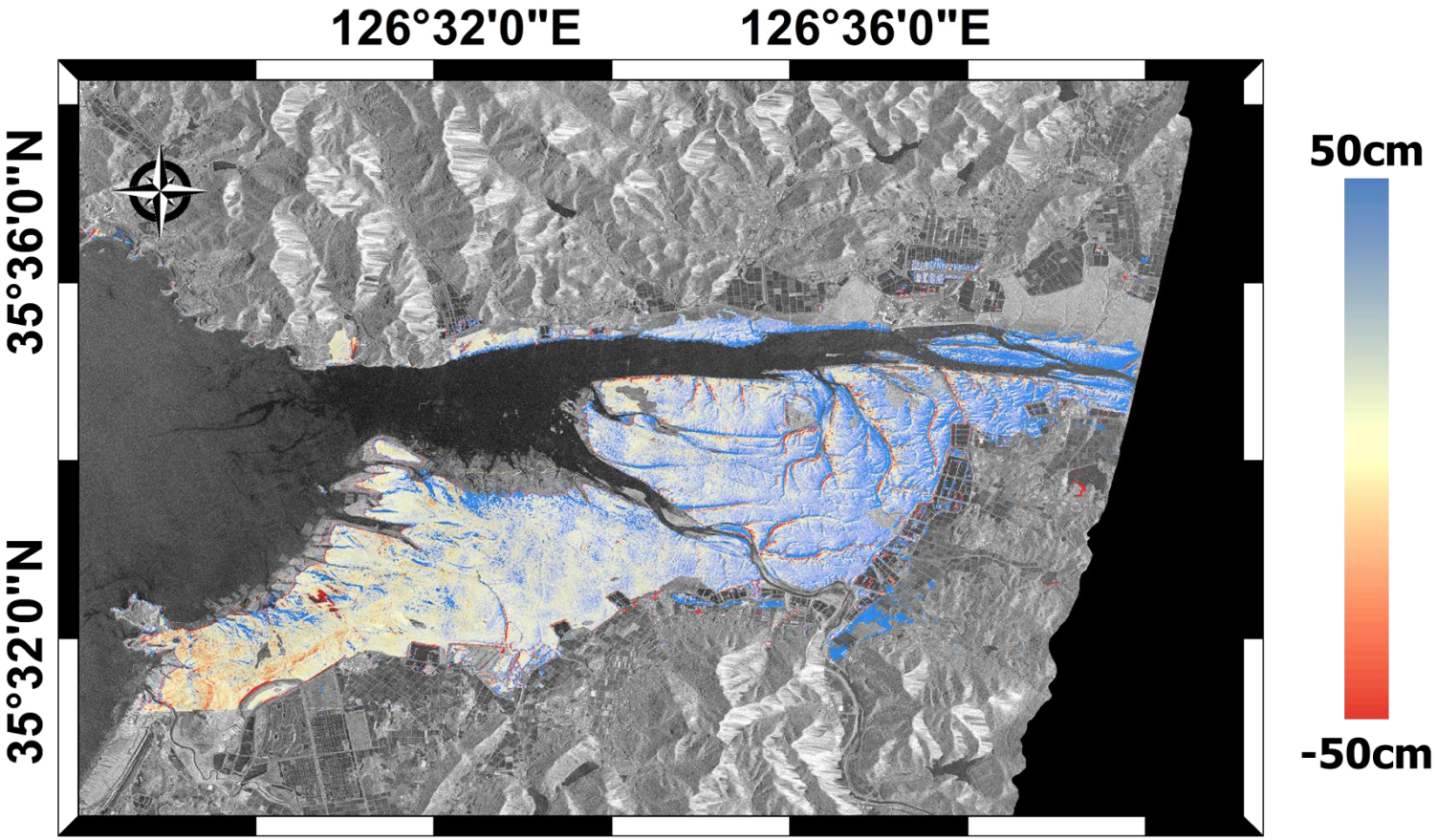

Fig. 12. Topographic change during summer in the Gomso bay.

From the previous estimation, two DEMs have error of 15 cm and 17 cm respectively. Height random error follows statistics thus, we can yield the co-variance of two DEM. Variance of summation of two population is expressed as summation of each variance. As a result, difference of DEM has standard deviation of 22 cm. We divided Gomso bay into five types from difference of DEM (1) more than 44 cm (2) less than 44 cm and more than 22cm (3) less than 22 cm and more than -22 cm (4) less than -22 cm and more than -44 cm (5) less than -44 cm. First and second types represented deposition zone whereas fourth and fifth types indicated erosion zone. Fig. 13 is the result of classification.

Deposition is dominant in the study area, particularly in head of the bay. There are many tidal bars in head of the bay where have fast deposition rates [41]. This region shows strong deposition signal with more than 30 cm topographic variation. The middle of the bay does not reflect significant topographic variation. Whereas, mouth region shows erosion pattern in with around 20 cm. This erosion pattern is well match with quantitative analysis conducted by waterline method [16] but other region do not have any significant erosion signal. This is because waterline method cannot provide high resolution with detail variation. In addition, it contains temporal error caused by stacking time-series optics data.

Fig. 14, on the other hand, does not show any significant pattern. This is because Doowoori is one of the stable tidal flat with low temporal topographic variation.

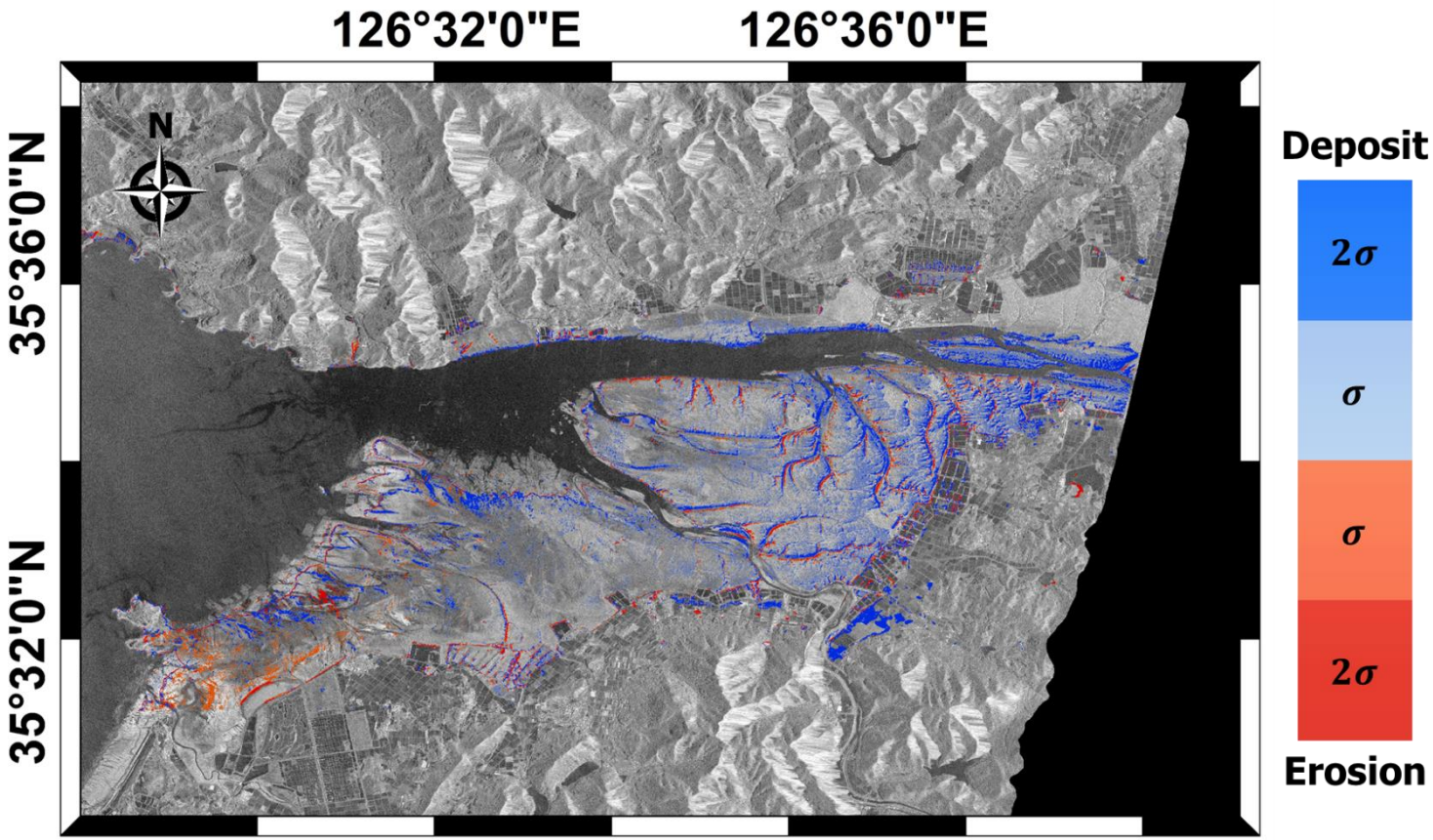

Fig. 13. Sedimentation pattern during June to September in the Gomso-bay.

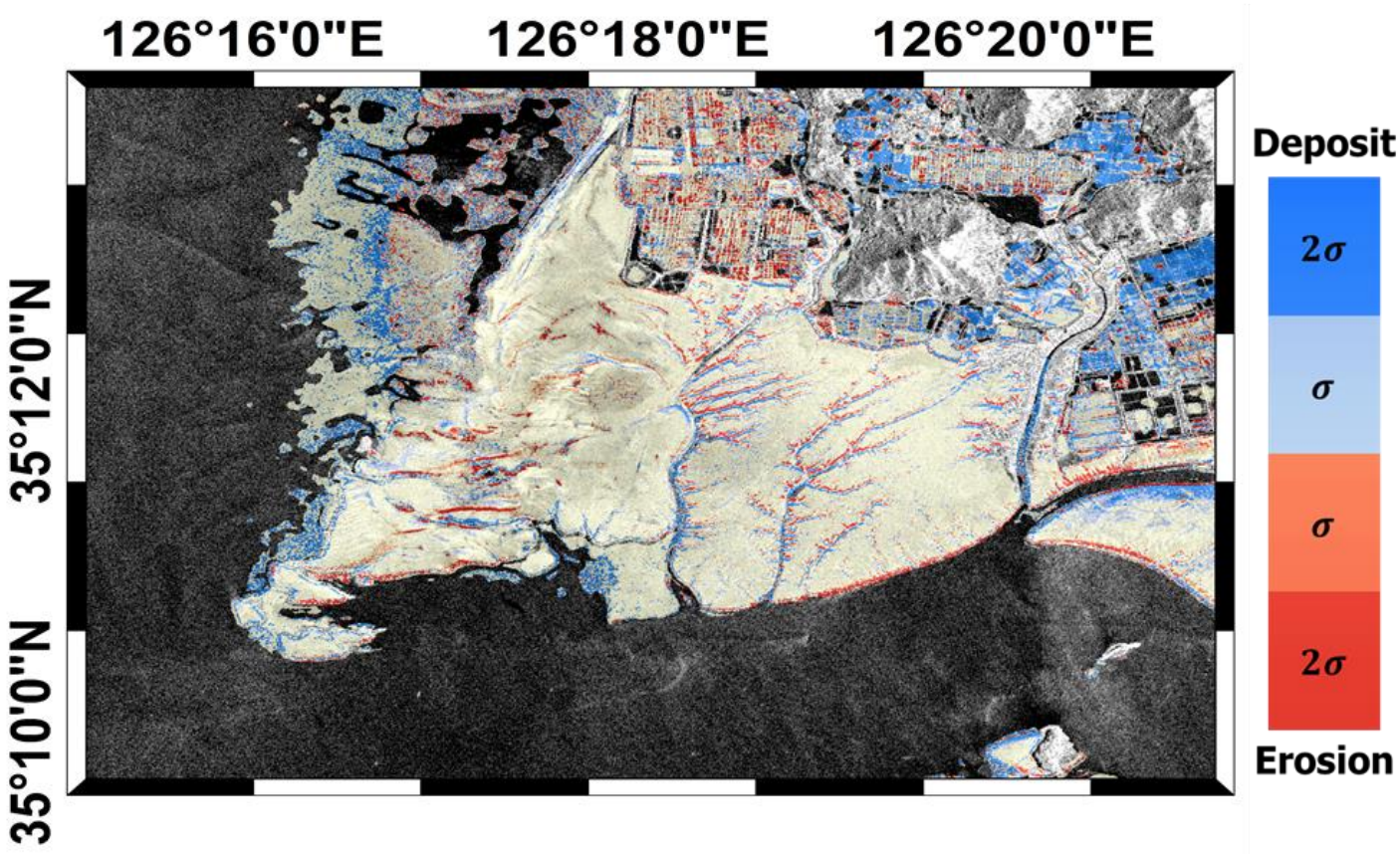

Fig. 14. Topographic change during summer in the Doowoori tidal flat.

5. Summary

A way to decide single pass In-SAR sensor formation for topography mapping in coastal area has primarily presented and discussed in this study. In tidal flats, based on two assumption (1) negligible volume decorrelation and (2) SAR backscattering coefficient is only function of incidence angle, we applied IEM to calculate SNR decorrelation in study area. Then, interferometric phase deviation was estimated from IEM and decorrelation equation with function of baseline and incidence angle. Combining both equations, we can estimate relative height error of DEM derived from In-SAR system as well as coherence.

Then, we found the optimum range to generate the fine topography map in study area using In-SAR where incidence angle is 31° and baseline is around 1170 m. In order to conserve detail topographic information, slope adaptivity is also important factor. Thus, local slope effect was considered for estimation of height accuracy.

Finally, the simulation result is then validated by comparing of interferograms derived from TanDEM-X data. The estimated coherence value and extracted from interferograms of TanDEM-X data are well matched as well as height error. This comparison provides that proposed model is possible to provide reliable estimation in tidal flat.

In this study, we applied proposed approach to estimation of height

accuracy of DEM derived from In-SAR. This estimation provide quantitative analysis based on decorrelation factor. Furthermore, proposed model also can be used to estimate In-SAR DEM error in surface scattering dominant fields like soil or sub-urban area. Then, we can find the adequate geometry of In-SAR to obtain best topographic information. In addition, this model can be applied to various wavelength and height system or even airborne system. Thus, it could provide the optimized In-SAR system to generate DEM in various situations.

Bibliography

[1] K. Reise, *Tidal flat ecology: an experimental approach to species interactions* vol. 54: Springer Science & Business Media, 2012.

[2] M. L. Parry, *Climate change 2007-impacts, adaptation and vulnerability: Working group II contribution to the fourth assessment report of the IPCC* vol. 4: Cambridge University Press, 2007.

[3] M. E. Assessment, "Ecosystems and human well-being: wetlands and water," *World resources institute, Washington, DC,* vol. 5, 2005.

[4] D. H. Song, X. H. Wang, X. M. Zhu, and X. W. Bao, "Modeling studies of the far-field effects of tidal flat reclamation on tidal dynamics in the East China Seas," *Estuarine Coastal and Shelf Science,* vol. 133, pp. 147-160, Nov 20 2013.

[5] Y. Hodoki and T. Murakami, "Effects of tidal flat reclamation on sediment quality and hypoxia in Isahaya Bay," *Aquatic Conservation-Marine and Freshwater Ecosystems,* vol. 16, pp. 555-567, Sep-Oct 2006.

[6] K. B. Gedan, M. L. Kirwan, E. Wolanski, E. B. Barbier, and B. R. Silliman, "The present and future role of coastal wetland vegetation in protecting shorelines: answering recent challenges to the paradigm," *Climatic Change,* vol. 106, pp. 7-29, May 2011.

[7] M. L. Kirwan, S. Temmerman, E. E. Skeehan, G. R. Guntenspergen, and S. Fagherazzi, "Overestimation of marsh vulnerability to sea level rise," *Nature Climate Change,* vol. 6, pp. 253-260, 2016.

[8] S. Fang, X. Jia, Q. Qian, J. Cui, G. Cagle, and A. Hou, "Reclamation history and development intensity determine soil and vegetation characteristics on

developed coasts," *Science of The Total Environment,* vol. 586, pp. 1263-1271, 2017.

[9] M. L. Kirwan and J. P. Megonigal, "Tidal wetland stability in the face of human impacts and sea-level rise," *Nature,* vol. 504, pp. 53-60, 2013.

[10] K. N. Mouritsen, L. T. Mouritsen, and K. T. Jensen, "Change of topography and sediment characteristics on an intertidal mud-flat following mass-mortality of the amphipod Corophium volutator," *Journal of the Marine Biological Association of the United Kingdom,* vol. 78, pp. 1167-1180, Nov 1998.

[11] B. H. Choe, D. J. Kim, J. H. Hwang, Y. Oh, and W. M. Moon, "Detection of oyster habitat in tidal flats using multi-frequency polarimetric SAR data," *Estuarine Coastal and Shelf Science,* vol. 97, pp. 28-37, Jan 20 2012.

[12] S. R. Phinn, C. Menges, G. J. E. Hill, and M. Stanford, "Optimizing remotely sensed solutions for monitoring, modeling, and managing coastal environments," *Remote Sensing of Environment,* vol. 73, pp. 117-132, Aug 2000.

[13] D. Mason, T. Scott, and S. Dance, "Remote sensing of intertidal morphological change in Morecambe Bay, UK, between 1991 and 2007," *Estuarine, Coastal and Shelf Science,* vol. 87, pp. 487-496, 2010.

[14] D. C. Mason, I. J. Davenport, R. A. Flather, and C. Gurney, "A digital elevation model of the inter-tidal areas of the Wash, England, produced by the waterline method," *International Journal of Remote Sensing,* vol. 19, pp. 1455-1460, May 20 1998.

[15] J. H. Ryu, J. S. Won, and K. D. Min, "Waterline extraction from Landsat TM data in a tidal flat - A case study in Gomso Bay, Korea," *Remote Sensing of*

Environment, vol. 83, pp. 442-456, Dec 2002.

[16] Z. Xu, D.-j. Kim, S. H. Kim, Y.-K. Cho, and S.-G. Lee, "Estimation of seasonal topographic variation in tidal flats using waterline method: A case study in Gomso and Hampyeong Bay, South Korea," *Estuarine, Coastal and Shelf Science,* vol. 183, pp. 213-220, 2016.

[17] H. F. Stockdon, A. H. Sallenger, J. H. List, and R. A. Holman, "Estimation of shoreline position and change using airborne topographic lidar data," *Journal of Coastal Research,* vol. 18, pp. 502-513, Sum 2002.

[18] J.-S. Won and S.-W. Kim, "ERS SAR interferometry for tidal flat DEM," in *Proc. of FRINGE 2003 Workshop, Frascati, Italy*, 2003.

[19] C. Wimmer, R. Siegmund, M. Schwabisch, and J. Moreira, "Generation of high precision DEMs of the Wadden Sea with airborne interferometric SAR," *Ieee Transactions on Geoscience and Remote Sensing,* vol. 38, pp. 2234-2245, Sep 2000.

[20] S.-K. Lee and J.-H. Ryu, "High-Accuracy Tidal Flat Digital Elevation Model Construction Using TanDEM-X Science Phase Data," *IEEE Journal of Selected Topics in Applied Earth Observations and Remote Sensing,* 2017.

[21] H. Greidanus, E. Huising, Y. Platschorre, R. Van Bree, D. Van Halsema, and E. Vaessen, "Coastal DEMs with cross-track interferometry," in *Geoscience and Remote Sensing Symposium, 1999. IGARSS'99 Proceedings. IEEE 1999 International*, 1999, pp. 2161-2163.

[22] A. P. Cracknell, "Remote sensing techniques in estuaries and coastal zones - an update," *International Journal of Remote Sensing,* vol. 20, pp. 485-496, Feb 15 1999.

[23] R. A. Davis Jr and R. W. Dalrymple, *Principles of tidal sedimentology*:

Springer Science & Business Media, 2011.

[24] R. Burgmann, P. A. Rosen, and E. J. Fielding, "Synthetic aperture radar interferometry to measure Earth's surface topography and its deformation," *Annual Review of Earth and Planetary Sciences,* vol. 28, pp. 169-209, 2000.

[25] E. Rodriguez and J. M. Martin, "Theory and Design of Interferometric Synthetic Aperture Radars," *Iee Proceedings-F Radar and Signal Processing,* vol. 139, pp. 147-159, Apr 1992.

[26] H. A. Zebker and J. Villasenor, "Decorrelation in Interferometric Radar Echoes," *Ieee Transactions on Geoscience and Remote Sensing,* vol. 30, pp. 950-959, Sep 1992.

[27] D. Just and R. Bamler, "Phase Statistics of Interferograms with Applications to Synthetic-Aperture Radar," *Applied Optics,* vol. 33, pp. 4361-4368, Jul 10 1994.

[28] M. Martone, B. Brautigam, P. Rizzoli, C. Gonzalez, M. Bachmann, and G. Krieger, "Coherence evaluation of TanDEM-X interferometric data," *Isprs Journal of Photogrammetry and Remote Sensing,* vol. 73, pp. 21-29, Sep 2012.

[29] J. S. Lee, A. R. Miller, and K. W. Hoppel, "Statistics of Phase Difference and Product Magnitude of Multi-Look Processed Gaussian Signals," *Waves in Random Media,* vol. 4, pp. 307-319, Jul 1994.

[30] J. S. Lee, K. W. Hoppel, S. A. Mango, and A. R. Miller, "Intensity and Phase Statistics of Multilook Polarimetric and Interferometric Sar Imagery," *Ieee Transactions on Geoscience and Remote Sensing,* vol. 32, pp. 1017-1028, Sep 1994.

[31] R. Touzi, A. Lopes, J. Bruniquel, and P. W. Vachon, "Coherence estimation

for SAR imagery," *Ieee Transactions on Geoscience and Remote Sensing,* vol. 37, pp. 135-149, Jan 1999.

[32] M. Gade, W. Alpers, C. Melsheimer, and G. Tanck, "Classification of sediments on exposed tidal flats in the German Bight using mufti-frequency radar data," *Remote Sensing of Environment,* vol. 112, pp. 1603-1613, Apr 15 2008.

[33] A. K. Fung and K. S. Chen, "An Update on the IEM Surface Backscattering Model," *Ieee Geoscience and Remote Sensing Letters,* vol. 1, pp. 75-77, Apr 2004.

[34] M. C. Dobson, F. T. Ulaby, M. T. Hallikainen, and M. A. Elrayes, "Microwave Dielectric Behavior of Wet Soil .2. Dielectric Mixing Models," *Ieee Transactions on Geoscience and Remote Sensing,* vol. 23, pp. 35-46, 1985.

[35] F. Gatelli, A. M. Guarnieri, F. Parizzi, P. Pasquali, C. Prati, and F. Rocca, "The Wave-Number Shift in Sar Interferometry," *Ieee Transactions on Geoscience and Remote Sensing,* vol. 32, pp. 855-865, Jul 1994.

[36] H. Lee and J. G. Liu, "Analysis of topographic decorrelation in SAR interferometry using ratio coherence imagery," *Ieee Transactions on Geoscience and Remote Sensing,* vol. 39, pp. 223-232, Feb 2001.

[37] S. Ryu, "Seasonal variation of sedimentary processes in a semi-enclosed bay: Hampyong bay, Korea," *Estuarine, Coastal and Shelf Science,* vol. 56, pp. 481-492, 2003.

[38] B. Y. Suk and C. Seungsoo, "Depositional Characteristics and Seasonal Change of Surface Sediment and Sedimentary Strucutre on the Doowoovi Tidal Flat, Southwestern Coast of Korea," *The Korean Journal of Petroleum*

Geology, vol. 10, 2004.

[39] G. Krieger, I. Hajnsek, K. P. Papathanassiou, M. Younis, and A. Moreira, "Interferometric Synthetic Aperture Radar (SAR) Missions Employing Formation Flying," *Proceedings of the Ieee,* vol. 98, pp. 816-843, May 2010.

[40] J. Chang and J. Choi, "Tidal-flat sequence controlled by Holocene sea-level rise in Gomso Bay, west coast of Korea," *Estuarine, Coastal and Shelf Science,* vol. 52, pp. 391-399, 2001.

[41] K. Choi, C. M. Hong, M. H. Kim, C. R. Oh, and J. H. Jung, "Morphologic evolution of macrotidal estuarine channels in Gomso Bay, west coast of Korea: Implications for the architectural development of inclined heterolithic stratification," *Marine Geology,* vol. 346, pp. 343-354, 2013.

[42] K. Choi, "Tidal rhythmites in a mixed-energy, macrotidal estuarine channel, Gomso Bay, west coast of Korea," *Marine Geology,* vol. 280, pp. 105-115, 2011.

국문 초록

갯벌에서의 퇴적과 침식은 간척사업이나 댐에 의한 해류의 변화나 기후변화에 의한 해수면 상승등에 의하여 빠르게 변화하고 있다. 이런 면에서 갯벌의 지형변화를 지속적으로 모니터링하는 것은 기후변화나 인위적인 토지사업 의하여 발생한 해류의 변화를 관찰할 수 있어 중요하다. 하지만, 현장 실측 조사를 통하여 갯벌의 지형변화를 관찰하는 것은 어려운 일이다. SAR 간섭 기법은 이런 어려움을 극복할 수 있는 도구로 넓은 영역의 변화를 관찰할 수 있는 도구다. 하지만, 갯벌 조간대에서 주기적으로 오고 나가는 밀물과 썰물은 In-SAR를 이용할 때에 큰 어려움을 발생시킨다. 이러한 문제는 Single-pass 시스템을 이용하여 극복할 수 있다. 그럼에도, 갯벌의 작은 경사와 년간 발생하는 작은 지형변화를 관찰하기 위해서는 극복해야할 것들이 남아있다. SAR를 이용하여 높은 정확도의 지형도를 제작하기위해서는 높은 긴밀도와 작은 Height of Ambiguity를 유지하여야 한다. 이런 파라미터들은 In-SAR 센서들 사이의 물리량에 의하여 결정되는 요소로, 기선거리와 입사각에 대한 함수로 나타낼 수 있다. 이 연구에서는 기존의 방정식과 IEM을 대입하여 최적의 지형도를 In-SAR에서 추출할 수 있는 기선거리와 입사각을 구하였다. TanDEM-X 시스템의 경우, 기선거리 1500 m 와 29도의 입사각에서 수직 오차 15 cm 미만의 높은 정확도의 지형도를 생성할 수 있다는 것을 계산을 통하여 추론하였다. 또한, 생성된 모델을 통하여 예측된 값들과 TanDEM-X에서 추출된 값을 비교하여 모델의 성능을 평가하였으며 최종적으로, 곰소만에서 계산된 두 장의 DEM을 이용하여 여름철 곰소만에서 발생하는 퇴적과 침식 작용을 분석해보았다.